Ultrafast thermoelastic dynamics of $HoMnO_3$ single crystals derived from femtosecond optical pump–probe spectroscopy

2011 New J. Phys. 13 053003

(http://iopscience.iop.org/1367-2630/13/5/053003)

New Journal of Physics
The open-access journal for physics

Ultrafast thermoelastic dynamics of $HoMnO_3$ single crystals derived from femtosecond optical pump–probe spectroscopy

H C Shih[1], L Y Chen[1], C W Luo[1,5], K H Wu[1], J-Y Lin[2], J Y Juang[1], T M Uen[1], J M Lee[3], J M Chen[3] and T Kobayashi[1,4]

[1] Department of Electrophysics, National Chiao Tung University, Hsinchu 300, Taiwan
[2] Institute of Physics, National Chiao Tung University (NCTU), Hsinchu 300, Taiwan
[3] National Synchrotron Radiation Research Center (NSRRC), Hsinchu 300, Taiwan
[4] Department of Applied Physics and Chemistry and Institute for Laser Science, The University of Electro-Communications, Chofugaoka 1-5-1, Chofu, Tokyo 182-8585, Japan
E-mail: cwluo@mail.nctu.edu.tw

New Journal of Physics **13** (2011) 053003 (11pp)
Received 25 November 2010
Published 3 May 2011
Online at http://www.njp.org/
doi:10.1088/1367-2630/13/5/053003

Abstract. In this paper, the photo-induced ultrafast thermoelastic dynamics of hexagonal $HoMnO_3$ single crystals has been studied by using optical pump–probe spectroscopy. The thermoelastic effect in the *ab*-plane of hexagonal $HoMnO_3$, associated with giant magnetoelastic coupling around the Néel temperature (T_N), is intimately correlated to the emergence of a negative component in the transient reflectivity changes ($\Delta R/R$) obtained in temperature-dependent pump–probe experiments. Moreover, the variation in the oscillation period in $\Delta R/R$ caused by a strain pulse propagating along the *c*-axis exhibits an abrupt drop around T_N, presumably due to the antiferromagnetic-ordering-induced changes in ferroelectricity.

[5] Author to whom any correspondence should be addressed.

Contents

1. Introduction

Multiferroic oxides have attracted a great deal of attention in recent years because of the strong coupling between the charge, spin, orbital, and lattice degrees of freedom and the accompanying rich and intriguing physics [1]–[8]. Since the relevant orderings can be manipulated through magnetoelectric coupling (the induction of magnetization by an electric field or of polarization by a magnetic field) [5, 6], multiferroic oxides are expected to have great potential for application in the fields of oxide electronics and spintronics, and also in green energy devices designed for reduced power consumption. Therefore, an understanding of the coupling between electric and magnetic ordering is at the heart of realizing these applications of multiferroic oxides. Due to the intrinsic integration and strong coupling between ferroelectricity and magnetism, however, the physics of multiferroicity is extremely complicated. For instance, the linear magnetoelectric effect that was thermodynamically described within the Landau theory framework [9] cannot be observed in $BiFeO_3$ owing to the cycloid antiferromagnetic (AFM) structure that even its crystal symmetry allows. Once the cycloid AFM structure is destroyed by a magnetic field, the linear magnetoelectric effect can be clearly observed in the case of $BiFeO_3$ [10]. In contrast, the linear magnetoelectric effect is forbidden in hexagonal manganites $HoMnO_3$ and thus the detailed mechanism of the electric field control of the magnetic phase remains unclear. Until recently, the origin of their magnetoelectric phenomenon has been further interpreted as due to the so-called magnetoelastic effect [11], which eventually leads to an effective coupling between electric dipole moment and magnetic moment by virtue of combining the elastic coupling between ferroelectric (FE) polarization and strain with magnetic anisotropy. However, all of these anisotropic couplings have never been simultaneously observed in a single measurement.

In the last two decades or so, many studies have demonstrated that ultrafast optical spectroscopy can provide valuable insights into the microscopic dynamics and the underlying functional responses in complex materials. In particular, the ability to simultaneously probe the evolution of multiple degrees of freedom in the time domain, as well as the coupling between them, has made pump–probe spectroscopy a unique and powerful tool for investigating the dynamical properties of multiferroics. For instance, Ogasawara *et al* [12] showed that the complex correlation between charge, lattice and spin in various ferromagnetic and ferrimagnetic compounds can be explicitly identified on different characteristic time scales by measuring the transient reflectivity or transmissivity changes.

In this study, we derived the ultrafast photo-induced electron and lattice dynamics of hexagonal $HoMnO_3$ (h-HMO) single crystals by using the wavelength-tunable femtosecond pump–probe technique. It was found that, around T_N, the anomalous thermoelastic effect in the ab-plane and that along the c-axis unambiguously couple with the AFM and FE orderings, as reflected in various components of the temperature-dependent transient reflectivity changes ($\Delta R/R$).

2. Experiments

The physical characteristics of the high-quality h-HMO single crystals used in this study have been described in detail previously [13]. Briefly, the h-HMO single crystals were grown by a traveling solvent optical floating zone method and examined by temperature-dependent magnetization measurements. For pump–probe measurements, we utilized a commercial mode-locked Ti:sapphire laser with 30 fs and tunable wavelengths from 740 to 800 nm ($h\nu = 1.68$–1.55 eV) with a spectrum width of 25 nm as the light source. The fluences of the pump beam and the probe beam were 0.18–0.79 and 0.05 μJ cm^{-2}, respectively. The pump beam was focused on the h-HMO single crystals at a spot with a diameter of 0.5 mm and the probe beam was focused on a spot with a diameter of 0.3 mm that overlapped the spot of the pump beam. The polarizations of the pump beam and the probe beam were perpendicular to each other and parallel to the ab-plane of the h-HMO single crystals (i.e. $E \perp c$-axis). Moreover, both beams were set in almost normal incidence. The transient reflectivity changes of the probe beam were detected by using a photodiode detector and a lock-in amplifier.

3. Results and discussion

3.1. Temperature- and wavelength-dependent $\Delta R/R$

Figure 1 shows the typical temperature-dependent $\Delta R/R$ obtained at various wavelengths. The rising part of the $\Delta R/R$ curve reflects the d–d excitation of carriers from e_{2g} band to a_{1g} band induced by the optical pump pulses. Thus, the number of excited carriers due to a nonthermal process is related to the amplitude of $\Delta R/R$ at zero delay time (see figure 3 [13]). After excitation, the hot electrons accumulated in the a_{1g} band start to release their energy through thermal processes, such as electron–phonon collisions [14]. During the electron–phonon collision processes, the energy transferred from the hot electrons may generate the thermoelastic effect and may further amplify the lattice vibrations. The above-mentioned relaxation processes ($t > 0$) as reflected in $\Delta R/R$ are frequently and phenomenologically described by fitting with the following equation [15],

$$\begin{aligned}\frac{\Delta R}{R}(\lambda, T, t) &= A_e(\lambda, T)e^{(-t/\tau_e)} + A_p(\lambda, T)(1 - e^{(-t/\tau_{p,r})})e^{-(t-\tau_{p,0})/\tau_{p,d}} \\ &\quad + A_n(\lambda, T)(1 - e^{-t/\tau_{n,r}})e^{-(t-\tau_{n,0})/\tau_{n,d}} + A_o(\lambda, T)e^{-t/\tau_o}\cos(\omega t - \phi). \qquad (1)\end{aligned}$$

The first term in the right-hand side of equation (1) represents the decay in the number $A_e(\lambda, T)$ of excited electrons with the relaxation time of τ_e. The second term represents the increase and decrease in the number $A_p(\lambda, T)$ of phonons with the rise time $\tau_{p,r}$ and decay time $\tau_{p,d}$, where $\tau_{p,0}$ is the starting time of phonon decay. Due to the electron–phonon coupling, the $\tau_{p,r}$ was set to be equal to τ_e in the data fitting. The number of excited electrons

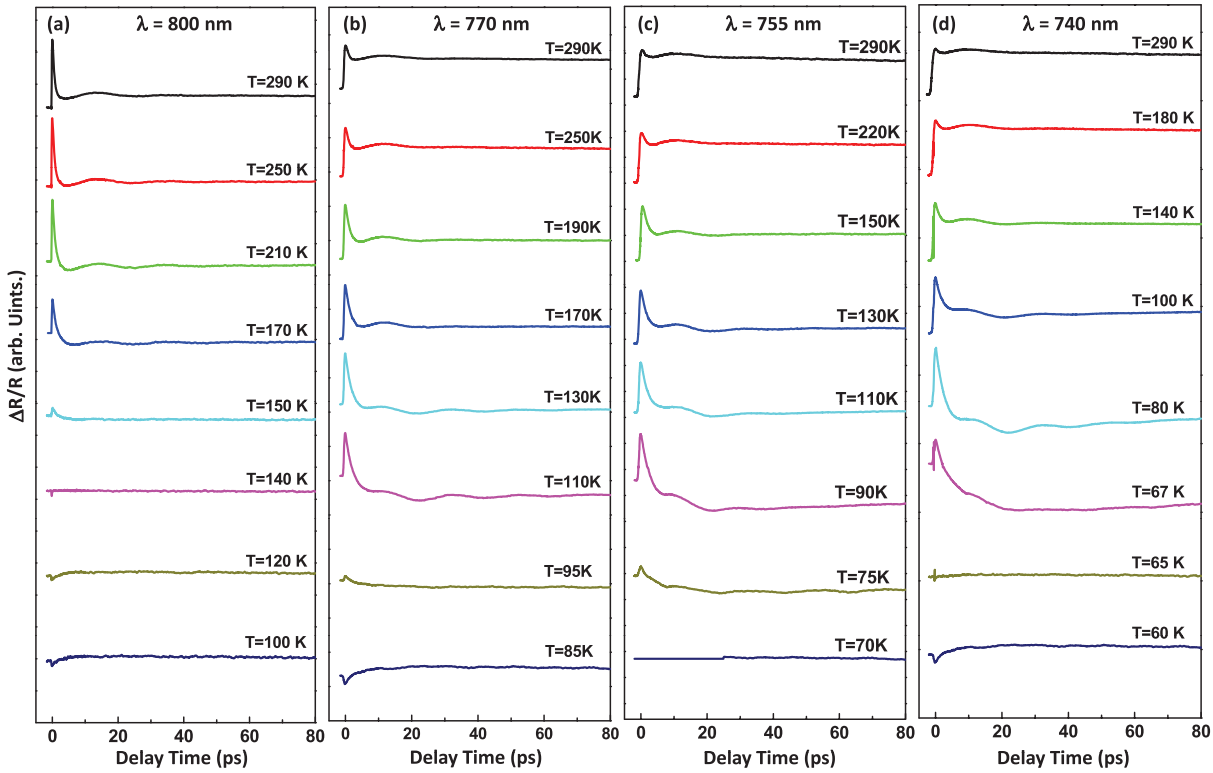

Figure 1. The photo-induced $\Delta R/R$ as a function of temperature at various wavelengths: (a) $\lambda = 800$ nm, (b) $\lambda = 770$ nm, (c) $\lambda = 755$ nm and (d) $\lambda = 740$ nm. The temperatures shown in this figure are the steady-state temperatures of samples.

decreases exponentially (dashed lines in figure 2) due to the electron–phonon collisions. In the meanwhile, the number of phonons increases initially to respond to the energy gain from the electron–phonon collisions (short dashed lines in figure 2) and then decays by losing energy to the environment. The third term describes the negative component associated with the magnetic ordering; $A_n(\lambda, T)$ is the strength of magnetic ordering, $\tau_{n,r}$ is the magnetic disordering time, $\tau_{n,d}$ is the magnetic reordering time and $\tau_{n,0}$ is the starting time of magnetic reordering. The final term describes the oscillation component associated with strain pulse propagation; $A_o(\lambda, T)$ is the amplitude of the oscillation component, τ_o is the damping time of the oscillation component, ω is the angular frequency of the oscillation component and ϕ is the initial phase of the oscillation component. Except for the oscillation term, equation (1) is consistent with the widely accepted three-temperature model [16, 17], which completely reveals the characteristics of the $\Delta R/R$ curves at $T > T_N$ and $T < T_N$, as shown in figure 2.

3.2. Attribution of the negative component in $\Delta R/R$

As shown in figure 1, the level of the amplitude of $\Delta R/R$ in the long decay time (>40 ps) regime decreases with decreasing temperature and even overshoots into the 'negative' territory. Thus, in order to describe the lower value of $\Delta R/R$ at $t > 5$ ps, an emerging 'negative component' is imposed as $A_n(\lambda, T)$ in equation (1) (see figure 2(b)). It is interesting to note that this negative

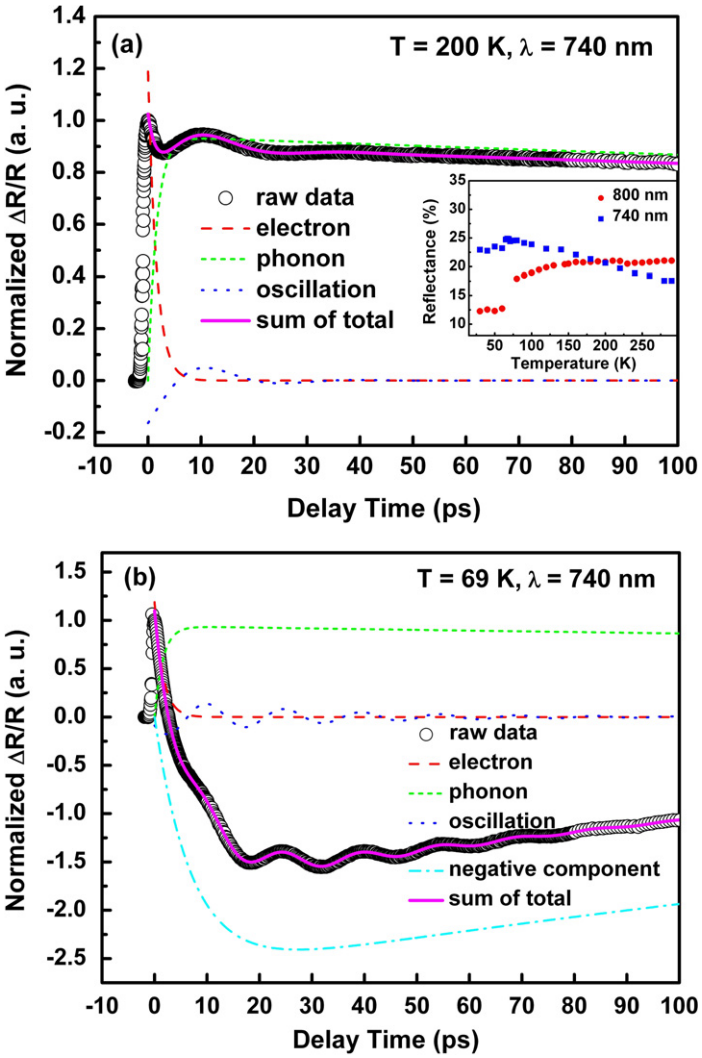

Figure 2. The selected $\Delta R/R$ curves at (a) 200 K and (b) 69 K are fitted by equation (1). Inset: the temperature-dependent reflectance at various wavelengths.

component grows gradually with decreasing temperature and exhibits a dramatic change while the temperature is approaching T_N. This characteristic is clearly demonstrated by the data point (solid squares) displayed in figure 3. Phenomenologically, a negative $\Delta R/R$ indicates that upon disturbance by the arrival of pump pulses at $t = 0$, something happens to make the reflectivity of the probe pulses drop to below its original magnitude. One of the possible reasons for this dramatic reduction in reflectivity is an abrupt increase in absorption, which might be realized if there is a sudden increase of the empty density of states (DOS) within the energy range of the probe beam. As indicated previously, in hexagonal rare-earth manganites, the energy difference between the a_{1g} and e_{2g} bands (E_{dd}) increases with decreasing temperature and is accompanied by a rather significant extra blueshift near T_N [13], [18]–[20]. After pumping, the electron–phonon scattering will raise the lattice temperature and push the Mn atoms back to the

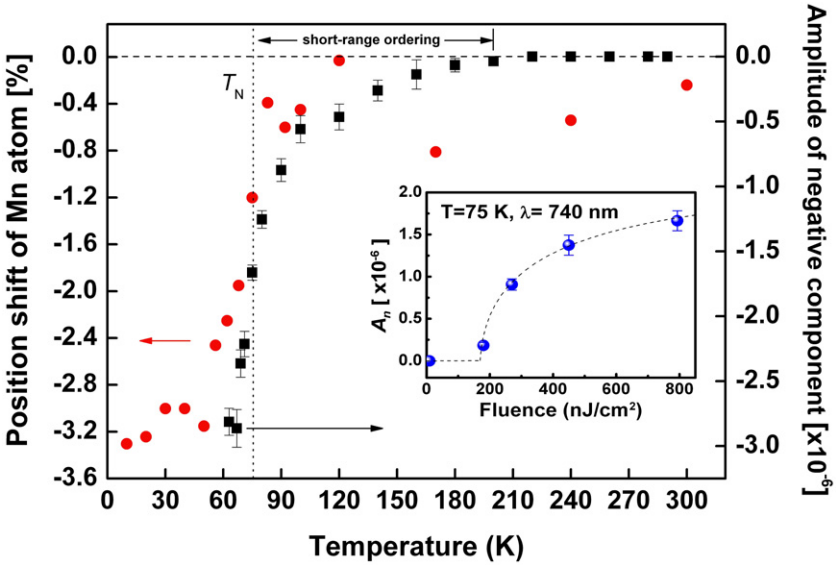

Figure 3. The amplitude of the negative component (solid squares) as a function of temperature. The solid circles are taken from [10]. Note: the T_N of $YMnO_3$ and $HoMnO_3$ are 70 and 76 K, respectively. Inset: the pumping fluence-dependent amplitude of the negative component A_n (740 nm, 75 K). The dashed line is a guide to the eyes. The temperatures shown in this figure are the steady-state temperatures of the samples.

position at higher temperatures and, in particular, disrupt the magnetic ordering. Consequently, a redshift of e_{2g} band with increasing temperature [13] will raise the available DOS in the a_{1g} band for absorbing more probe photons ($\Delta A > 0$) with the same wavelength and lead to the emergence of negative $\Delta R/R$ ($\Delta R \propto -\Delta A$ and $A_n(\lambda, T) \neq 0$ in equation (1)). Moreover, after a certain pumping fluence, $A_n(\lambda, T)$ increases with increasing pumping fluences and saturates at high fluences, as shown in the inset of figure 3.

We note that the temperature dependence of the amplitude of negative $\Delta R/R$ [$A_n(\lambda, T)$] is very similar to the displacement of Mn atoms (solid circles in figure 3) that was revealed by high-resolution neutron diffraction measurements recently [11]. In [11], it has been pointed out that the drastic position shift of the Mn atoms is directly associated with the magnetic ordering of the Mn moments and is regarded as strong evidence of magnetoelastic coupling. The large position shift of the Mn atoms, in turn, produces a further coupling to electric dipole moments [3] and changes the electronic structure of the system. Although it might appear coincident, the intimate similarity between the anomalous increase in the amplitude of the negative component of $\Delta R/R$ and the large displacement of Mn atoms around T_N (in figure 3) strongly suggests that they originate from the same magnetoelastic effect. Namely, the dramatic changes in amplitude of the negative component around T_N are due to disruption of the established long-range AFM ordering and the accompanying retraction of the magnetoelastic effect. Moreover, it is noted that the onset of the negative $\Delta R/R$ component appearing at temperatures well above T_N is attributed to the emergence of short-range AFM ordering [13].

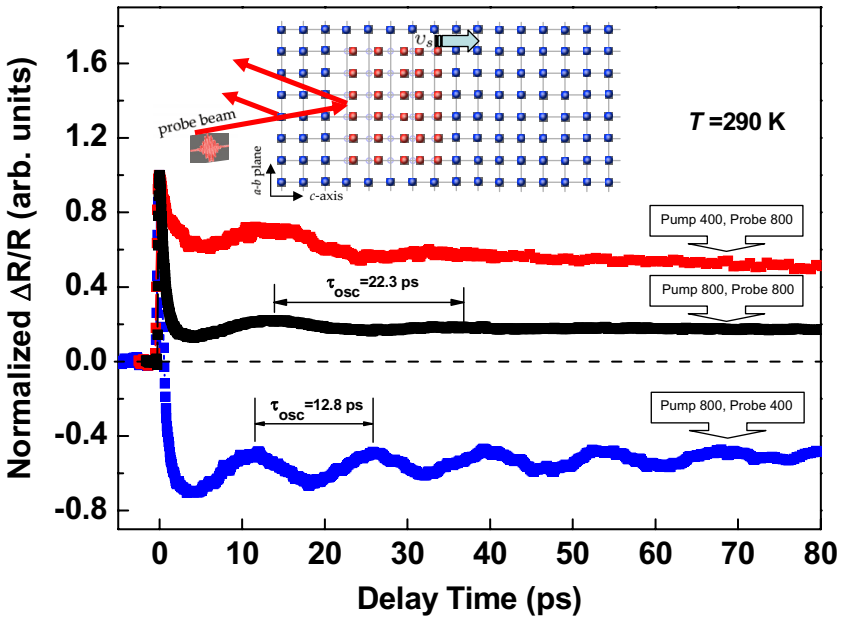

Figure 4. The photo-induced $\Delta R/R$ at various pump and probe wavelengths. Inset: schematic illustration of the oscillated $\Delta R/R$ due to a strain pulse.

3.3. Attribution of the oscillation component in $\Delta R/R$

Another interesting feature appearing in all of the $\Delta R/R$ curves is the damped oscillations (see the dotted lines in figure 2), which are described by the last term of equation (1) and have been ubiquitously observed in various materials. Thomsen *et al* [21, 22] termed these damped oscillations as the coherent acoustic phonons (CAP) induced by the electronic and lattice stresses. In their model, the stress tensor contributed by the nonthermal and thermal origins can be written as $\sigma_{ij} = \sigma_e + \sigma_p$, with σ_e corresponding to the electronic stress and σ_p corresponding to the thermoelastic stress, respectively. In an isotropic medium, the thermoelastic stress can be expressed as $\sigma_p = -3K\beta\Delta T_l$, where K is the bulk elastic modulus, ΔT_l is the lattice temperature rise and β is the linear thermal-expansion coefficient. In this model [22], the oscillation of $\Delta R/R$ is caused by the interference between the probe beams reflected from the crystal surface and the rear interface of the propagating strain pulse with the modulated dielectric constant (or FE ordering), as illustrated schematically in the inset of figure 4. The changes in reflectivity due to the strain can be obtained by solving the Maxwell equations and the closed-form formula for $\Delta R/R$ is as follows [22],

$$\frac{\Delta R(t)}{R} \propto \cos\left(\frac{4\pi n v_s t}{\lambda} - \phi\right) e^{-v_s t/\xi}, \tag{2}$$

where λ is the wavelength of the probe pulses, n is the refractive index of samples, v_s is the speed of sound propagated in the medium and ξ is the penetration depth of probe pulses. Figure 4 shows the typical $\Delta R/R$ curves obtained by using different combinations of pump and probe wavelengths. It is evident that the frequency of the damped oscillations is solely dependent on the wavelength of the probe beam and is rather insensitive to that of the pump beam, which is

consistent with the essential features of CAP generation described by the simplified equation,

$$\omega = \frac{4\pi n v_s}{\lambda}. \tag{3}$$

Figure 5(a) shows the temperature dependence of the oscillation period τ_{osc} probed by using various wavelengths. Here, τ_{osc} is defined as $\tau_{osc} = 2\pi/\omega$ with ω obtained by fitting the data with equation (1). At room temperature, the τ_{osc} at 740 nm is larger than the τ_{osc} at 800 nm, which is the opposite of the prediction of $\tau_{osc} = \lambda/2nv_s$. Due to the increase in reflectance at 740 nm and the decrease in reflectance at 800 nm with decreasing temperatures shown in the inset of figure 2(a), the wavelength range from 800 nm (1.55 eV) to 740 nm (1.68 eV) is just located at the absorption peak of the optical conductivity spectra [20]. The giant difference between the optical conductivity (σ_1) values at 800 nm and 740 nm and the higher reflectance at 800 nm further leads to $(n_{800\,nm}/n_{740\,nm}) > (800\,nm/740\,nm)$.[6] With constant v_s, therefore, $\tau_{osc,800\,nm}$ would be smaller than $\tau_{osc,740\,nm}$. This result was also observed for $LuMnO_3$ by Lim *et al* [23]. Moreover, the difference between $\tau_{osc,800\,nm}$ and $\tau_{osc,740\,nm}$ decreases with decreasing temperature owing to the $n_{740\,nm}$ getting closer to $n_{800\,nm}$ (see the inset of figure 2(a)) (see footnote 6).

It is evident that, for all the probed wavelengths, τ_{osc} appears to decrease only slightly with decreasing temperature, which is consistent with a similar pump–probe spectroscopy study on hexagonal $LuMnO_3$ reported by Jang *et al* [15] and can be interpreted as due to the increase in rigidity of the isostructure lattice as the temperature is lowered. The shortest accessible probe wavelength in our system was 740 nm, which was the only wavelength to delineate such a dramatic change in τ_{osc} for temperatures below T_N. According to equation (3), τ_{osc} is a function of the refractive index n of probe pulses and the sound velocity. However, at a wavelength of 740 nm, $\Delta\, n_{69-100\,K}/n_{100\,K}$ is about 2.7% (see footnote 6), which cannot explain the variation in -30% in $\Delta\, \tau_{osc,69-100\,K}/\tau_{osc,100\,K}$. Therefore, such significant shrinkage of τ_{osc} around T_N is most probably dominated by the dramatic increase in v_s along the c-axis owing to the stiffness of the lattice at low temperatures, which is consistent with the Lim *et al* results for $LuMnO_3$ [23]. This strongly indicates that the propagation of a strain pulse with modulation of the dielectric constant along the c-axis should be affected by the FE properties with the FE polarization along the c-axis below T_c [3]. Indeed, the temperature-dependent dielectric properties of $HoMnO_3$ are drastically affected by the emergence of AFM ordering around T_N [3]. In any case, the AFM ordering in the *ab*-plane also influences the temperature-dependent oscillation period of $\Delta R/R$ along the c-axis through the magnetic–elastic coupling and then the elastic–ferroelectric coupling.

According to equation (2), the dephasing time τ_0 is proportional to the penetration depth ξ of probe pulses and the inverse sound velocity v_s, which is wavelength independent. At the same temperature, e.g. room temperature, $\tau_{0,800\,nm}$ is larger than $\tau_{0,740\,nm}$ because the penetration depth at 800 nm is larger than that at 740 nm in lossy media [24]. For all of the probing wavelengths, τ_0 almost remains constant above 180 K, which is associated with the starting temperature of short-range AFM ordering [13], as shown in figure 5(b) and the inset. With decreasing temperature, a significant increase in τ_0 at 740 nm is clearly observed around T_N. To figure out this phenomenon, we consider the attenuation constant as a function of the dielectric constant (ε_1 and ε_2) in lossy media [24]. However, the shrinkage of penetration depth caused by a

[6] Estimated from the temperature-dependent reflectance in the inset of figure 2(a) by the Fresnel equation at near normal incidence.

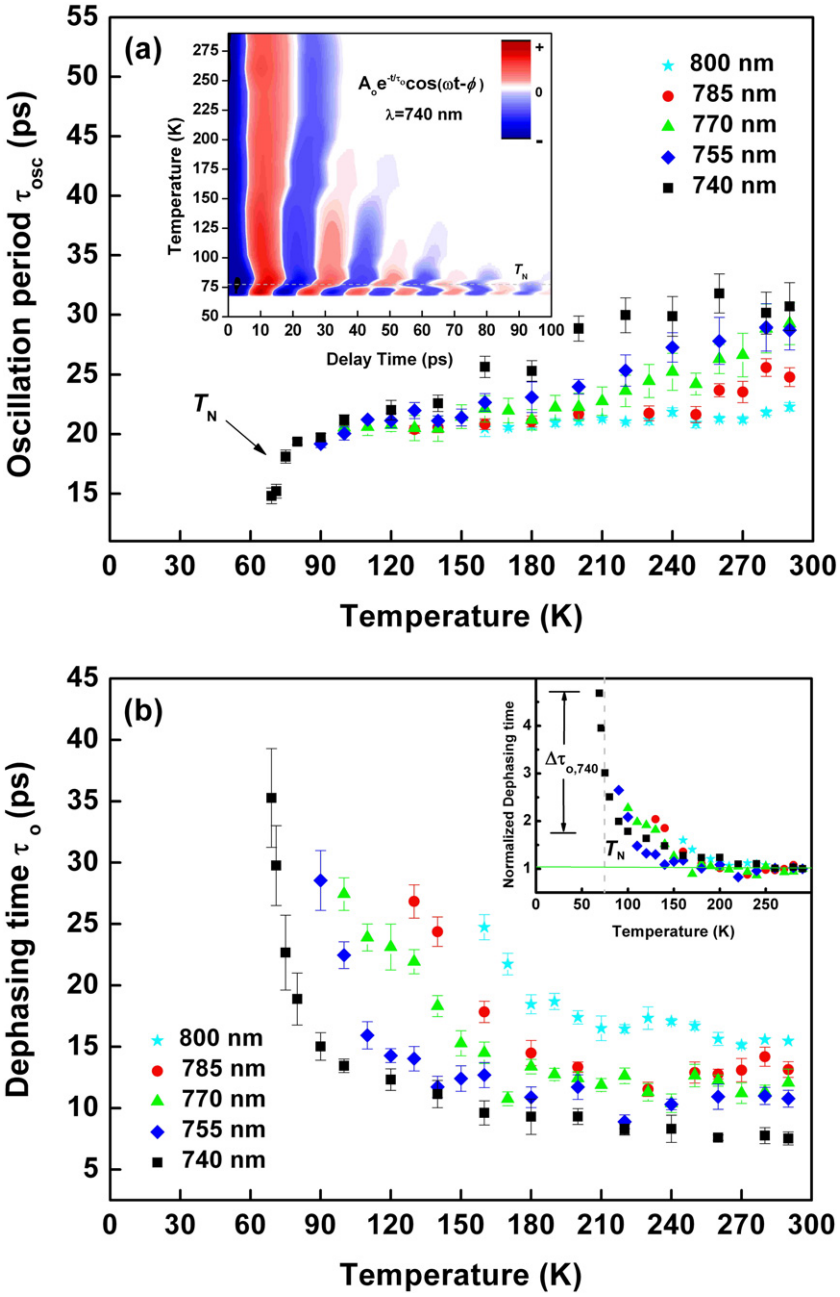

Figure 5. (a) The temperature-dependent oscillation period in $\Delta R/R$ at various wavelengths. Inset: the evolution of the oscillation component in $\Delta R/R$ at various temperatures. (b) The temperature-dependent dephasing time of the oscillation component in $\Delta R/R$ at various wavelengths. Inset: the normalized dephasing time as a function of temperature at various wavelengths. The temperatures shown in this figure are the steady-state temperatures of samples.

decrease of ε_1 at 1.68 eV (740 nm) [20] and an increase of ε_2 (estimated from the blueshift of σ_1 spectra in [20] through Kramers–Kronig relation) around T_N cannot explain the large enhancement ($\Delta\ \tau_{0,69-100\,K}/\tau_{0,100\,K} = 162\%$) in the dephasing time τ_0. Thus, this dramatic

growth of τ_0 around T_N should be dominated by the temperature-dependent v_s. Namely, v_s increases with decreasing temperature owing to the stiffness of the lattice at low temperatures, and it even overshoots around T_N owing to AFM ordering [23], which is consistent with the conclusion on the shrinkage of τ_{osc} around T_N. As mentioned before, Lee *et al* [11] in their neutron diffraction experiments also observed extra displacement of the rare-earth and oxygen atoms along the *c*-axis at T_N. On the basis of the magnetic-ordering-induced atomic displacement, it was argued that the observed magnetoelastic effect is the primary origin of the eventual magnetoelectric phenomenon in this intriguing class of materials.

4. Conclusion

In the present study, we have measured temperature-dependent transient reflectivity changes in hexagonal $HoMnO_3$ single crystals to study the photo-induced ultrafast thermoelastic dynamics. The emergence of AFM ordering of Mn^{3+} ions at T_N was clearly delineated in the temperature-dependent evolution of the negative component in $\Delta R/R$ caused by the thermal strain induced by the incident pump beam, which might be the result of a redshift in the *d–d* transition. The oscillation period and dephasing time in $\Delta R/R$ caused by the strain pulse propagating along the *c*-axis also exhibit a similar dramatic change around the AFM ordering temperature, indicating that an accompanying variation in FE ordering might have occurred simultaneously.

Acknowledgments

We thank the National Science Council of the Republic of China, Taiwan for financial support of this research under contract numbers NSC98-2112-M-009-006-MY3, NSC96-2923-M-009-001-MY3 and NSC98-2112-M-009-008-MY3, and the Grant MOE ATU program at NCTU.

References

[1] Eerenstein W, Mathur N D and Scott J F 2006 *Nature* **442** 759
[2] Spaldin N A and Fiebig M 2005 *Science* **309** 391
[3] dela Cruz C, Yen F, Lorenz B, Wang Y Q, Sun Y Y, Gospodinov M M and Chu C W 2005 *Phys. Rev.* B **71** 060407
[4] Lee S, Pirogov A, Han J H, Park J-G, Hoshikawa A and Kamiyama T 2005 *Phys. Rev.* B **71** 180413
[5] Lottermoser T, Lonkai T, Amann U, Hohlwein D, Ihringer J and Fiebig M 2004 *Nature* **430** 541
[6] Cheong S-W and Mostovoy M 2007 *Nat. Mater.* **6** 13
[7] Huang Z J, Cao Y, Sun Y Y, Xue Y Y and Chu C W 1997 *Phys. Rev.* B **56** 2623
[8] Lorenz B, Litvinchuk A P, Gospodinov M M and Chu C W 2004 *Phys. Rev. Lett.* **92** 087204
[9] Wang K F, Liu J-M and Ren Z F 2009 *Adv. Phys.* **58** 321
[10] Popov Yu F, Zvezdin A K, Vorob'ev G P, Kadomtseva A M, Murashev V A and Rakov D N 1993 *JETP Lett.* **57** 69
[11] Lee S 2008 *Nature* **451** 805
[12] Ogasawara T, Ohgushi K, Tomioka Y, Takahashi K S, Okamoto H, Kawasaki M and Tokura Y 2005 *Phys. Rev. Lett.* **94** 087202
[13] Shih H C, Lin T H, Luo C W, Lin J-Y, Uen T M, Juang J Y, Wu K H, Lee J M, Chen J M and Kobayashi T 2009 *Phys. Rev.* B **80** 024427
[14] Ruello P, Zhang S, Laffez P, Perrin B and Gusev V 2009 *Phys. Rev.* B **79** 094303
[15] Jang K-J, Lim J, Ahn J, Kim J-H, Yee K-J, Ahn J S and Cheong S-W 2010 *New J. Phys.* **12** 023017

[16] Averitt R D and Taylor A J 2002 *J. Phys.: Condens. Matter* **14** R1357
[17] Müller G M 2009 *Nat. Mater.* **8** 56
[18] Souchkov A B, Simpson J R, Quijada M, Ishibashi H, Hur N, Ahn J S, Cheong S W, Millis A J and Drew H D 2003 *Phys. Rev. Lett.* **91** 027203
[19] Choi W S, Moon S J, Seo S S A, Lee D, Lee J H, Murugavel P, Noh T W and Lee Y S 2008 *Phys. Rev.* B **78** 054440
[20] Rai R C, Cao J, Musfeldt J L, Kim S B, Cheong S-W and Wei X 2007 *Phys. Rev.* B **75** 184414
[21] Thomsen C, Strait J, Vardeny Z, Maris H J, Tauc J and Hauseru J J 1984 *Phys. Rev. Lett.* **53** 989
[22] Thomsen C, Grahn H T, Maris H J and Tauc J 1986 *Phys. Rev.* B **34** 4129
[23] Lim D, Averitt R D, Demsar J, Taylor A J, Hur N and Cheong S W 2003 *Appl. Phys. Lett.* **83** 4800
[24] Cheng D K 1989 *Field and Wave Electronmagnetics* (Reading, MA: Addison-Wesley)